

AD-A157 498

THE INHOMOGENEOUS LIGHT SHIFT IN ALKALI ATOMS(U)
AEROSPACE CORP EL SEGUNDO CA CHEMISTRY AND PHYSICS LAB
J C CAMPARO ET AL. 24 JUN 85 TR-0084A(5945-05)-6
SD-TR-85-19 F04701-83-C-0084 F/G 7/4

1/1

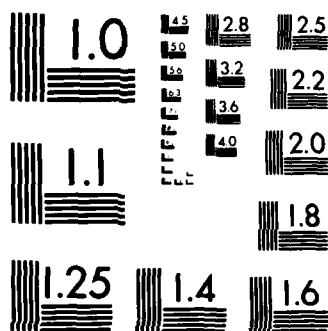
UNCLASSIFIED

F/G 7/4

NL

END

• 34. **Med D**



MICROCOPY RESOLUTION TEST CHART
NBS 1963-A

The Inhomogeneous Light Shift in Alkali Atoms

J. C. CAMPARO, R. P. FRUEHOLZ, and C. H. VOLK
Chemistry and Physics Laboratory
Laboratory Operations
The Aerospace Corporation
El Segundo, CA 90245

24 June 1985

APPROVED FOR PUBLIC RELEASE;
DISTRIBUTION UNLIMITED

AD-A157 498

DTIC FILE COPY

Prepared for
SPACE DIVISION
AIR FORCE SYSTEMS COMMAND
Los Angeles Air Force Station
P.O. Box 92960, Worldway Postal Center
Los Angeles, CA 90009-2960

DTIC
RECEIVED
AUG 2 1985
1

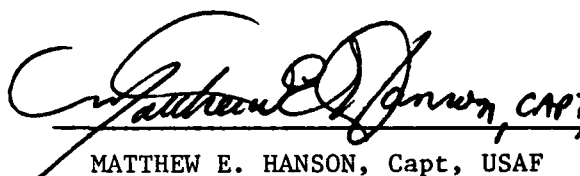
85 7 23 045

This report was submitted by The Aerospace Corporation, El Segundo, CA 90245, under Contract No. F04701-83-C-0084 with the Space Division, P.O. Box 92960, Worldway Postal Center, Los Angeles, CA 90009. It was reviewed and approved for The Aerospace Corporation by S. Feuerstein, Director, Chemistry and Physics Laboratory.

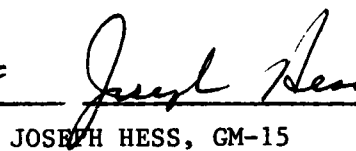
Capt Matthew E. Hanson, YEZ, was the project officer for the Mission-Oriented Investigation and Experimentation (MOIE) Program.

This report has been reviewed by the Public Affairs Office (PAS) and is releasable to the National Technical Information Service (NTIS). At NTIS, it will be available to the general public, including foreign nationals.

This technical report has been reviewed and is approved for publication. Publication of this report does not constitute Air Force approval of the report's findings or conclusions. It is published only for the exchange and stimulation of ideas.


MATTHEW E. HANSON, Capt, USAF

Ch, Satellite Development Branch
SD/YEVS


JOSEPH HESS, GM-15

Director, AFSTC West Coast Office
AFSTC/WCO OL-AB

UNCLASSIFIED

SECURITY CLASSIFICATION OF THIS PAGE (When Data Entered)

REPORT DOCUMENTATION PAGE		READ INSTRUCTIONS BEFORE COMPLETING FORM
1. REPORT NUMBER SD-TR-85-19	2. GOVT ACCESSION NO.	3. RECIPIENT'S CATALOG NUMBER
4. TITLE (and Subtitle) THE INHOMOGENEOUS LIGHT SHIFT IN ALKALI ATOMS		5. TYPE OF REPORT & PERIOD COVERED
7. AUTHOR(s) James C. Camparo, Robert P. Frueholz, and Charles H. Volk		6. PERFORMING ORG. REPORT NUMBER TR-0084A(5945-05)-6
9. PERFORMING ORGANIZATION NAME AND ADDRESS The Aerospace Corporation El Segundo, Calif. 90245		8. CONTRACT OR GRANT NUMBER(s) F04701-83-C-0084
11. CONTROLLING OFFICE NAME AND ADDRESS Space Division Los Angeles Air Force Station Los Angeles, Calif. 90009-2960		10. PROGRAM ELEMENT, PROJECT, TASK AREA & WORK UNIT NUMBERS
14. MONITORING AGENCY NAME & ADDRESS (if different from Controlling Office)		12. REPORT DATE 24 June 1985
		13. NUMBER OF PAGES 40
		15. SECURITY CLASS. (of this report) Unclassified
16. DISTRIBUTION STATEMENT (of this Report) Approved for public release; distribution unlimited.		15a. DECLASSIFICATION/DOWNGRADING SCHEDULE
17. DISTRIBUTION STATEMENT (of the abstract entered in Block 20, if different from Report)		
18. SUPPLEMENTARY NOTES		
19. KEY WORDS (Continue on reverse side if necessary and identify by block number) AC Stark effect, Atomic clocks, Atomic line shapes, Light shifts.		
20. ABSTRACT (Continue on reverse side if necessary and identify by block number) The dynamic Stark shift of an inhomogeneously broadened spectral transition has been studied. Our measurements show a shift in the observed 87Rb ground-state hyperfine transition, which has a nonlinear dependence on light intensity when the conditions for inhomogeneous broadening are met. The nonlinearity is the result of light-intensity gradients in the signal volume, which produce an inhomogeneously broadened asymmetric microwave transition. We show that our measurements are in full agreement with the		

DD FORM 1473
(FACSIMILE)

UNCLASSIFIED

SECURITY CLASSIFICATION OF THIS PAGE (When Data Entered)

UNCLASSIFIED

SECURITY CLASSIFICATION OF THIS PAGE(When Data Entered)

19. KEY WORDS (Continued)

20. ABSTRACT (Continued)

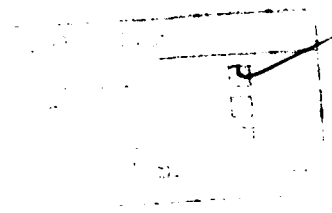
second-order perturbation-theory treatment of light-induced energy-level shifts, when the effects of inhomogeneities are properly taken into consideration. The effects of inhomogeneous broadening must be carefully considered when one extracts oscillator strengths from light-shift data, or performs high-precision laser spectroscopy. Original Supplied

UNCLASSIFIED

SECURITY CLASSIFICATION OF THIS PAGE(When Data Entered)

ACKNOWLEDGMENTS

We wish to thank William Happer of Princeton University for suggesting inhomogeneous broadening as the likely cause of our nonlinear light-shift data. In addition, we would like to thank S. K. Karuza and F. J. Voit for help with the microwave electronics.



CONTENTS

ACKNOWLEDGMENTS.....	1
I. INTRODUCTION.....	5
II. EXPERIMENTAL PROCEDURE.....	7
III. RESULTS.....	11
A. Light-Shift Measurements.....	11
B. Line Shape Measurements.....	14
IV. MODEL OF THE INHOMOGENEOUS LIGHT SHIFT.....	17
A. The Local Density Matrix.....	19
B. The Microwave Rabi Frequency.....	23
C. The Pumping Rate and Light Shift.....	24
V. DISCUSSION.....	27
VI. CONCLUSIONS.....	35
REFERENCES.....	37
APPENDIX: THE POTENTIAL FOR MOTIONAL AVERAGING OF SPATIAL INHOMOGENEITIES.....	39

FIGURES

1. Experimental Arrangement.....	8
2. Rb Hyperfine Transitions Observed in Transmission of the Laser Light.....	12
3. Experimental Results of the Light Shift versus Incident-Laser Intensity.....	13
4. Experimental Results of the Microwave Line Shape Measurements.....	15
5. Schematic Energy Level Diagram of ^{87}Rb	18
6. Calculated Resonant Microwave Line Shapes in the TE_{111} Microwave Cavity for Low and High Laser Intensity.....	28
7. Calculated Resonant Microwave Line Shapes in a Fictitious Microwave Cavity with Constant rf Magnetic Field for Low and High Laser Intensity.....	29
8. Calculated Inhomogeneous Light Shift in a TE_{111} Microwave Cavity for Several Detunings of the Laser.....	30
9. Calculated Inhomogeneous Light Shift in a Fictitious Microwave Cavity with Constant rf Magnetic Field for Several Detunings of the Laser.....	31

TABLE

1. Calculation Parameters.....	32
--------------------------------	----

I. INTRODUCTION

It has been known for quite some time that the near-resonant interaction between electromagnetic fields and atomic or molecular systems can lead to level shifts and splittings of the system under study.¹ When the field is sufficiently weak, the shift of the energy levels is quadratic in the field strength; when the field is strong, the shift is linear in the field strength. The correct dependence of the shift on field strength is very important when one performs high-resolution spectroscopy, or uses the field effect to accurately measure transition dipole matrix elements.² However, it is equally important to consider the effects of inhomogeneities when performing these measurements, since optically produced inhomogeneous broadening can drastically affect the observed shift.

Inhomogeneous effects can be easily observed and studied in hyperfine optical pumping experiments of alkali atoms, where the atom can be considered as essentially "frozen in place" because of the presence of buffer gas.³ In these experiments the level shift is referred to as the light shift due to virtual transitions, since the optical field produces a shift observed in a microwave or rf resonance. These shifts were first discussed by Barrat and Cohen-Tannoudji,⁴ and then treated semiclassically by Happer and Mathur.⁵ The light shift is of considerable importance in a number of devices such as frequency standards, optically pumped magnetometers, and masers; and although inhomogeneous effects have been discussed,^{6,7} no comprehensive experimental study of an inhomogeneous light shift has been undertaken.

We report here measurements on the level shifts in the ground-state ^{87}Rb (rubidium) hyperfine levels induced by laser radiation approximately in resonance with the transition from the ground state to the first excited state, $5^2\text{S}_{1/2} - 5^2\text{P}_{1/2}$. These shifts are deduced by measuring the center frequency of the ground-state hyperfine resonance as a function of incident-laser intensity. When inhomogeneous broadening is present, observed as an asymmetry in the hyperfine resonance line, the center frequency is found to be

a nonlinear function of the light intensity. We find that this nonlinearity is entirely consistent with a second-order perturbation treatment of the light shift, and can be explained on the basis of light-intensity gradients in the cell.

II. EXPERIMENTAL PROCEDURE

The experimental apparatus is shown schematically in Fig. 1. A glass absorption cell that contains an excess of Rb metal and N_2 at 10 Torr is situated in a TE_{111} microwave cavity tuned to the ^{87}Rb ground-state hyperfine transition frequency.⁸ The Rb is in its natural isotopic abundance, 27.2% ^{87}Rb and 72.8% ^{85}Rb ; the N_2 is present in order to quench the Rb fluorescence, and to act as a buffer to reduce the effect of collisions with the cell walls. A static magnetic field of about 300 mG is applied parallel to the cavity axis in order to define the quantization axis, and to split the Zeeman levels so that only the 0-0 transition is induced by the microwaves. The cavity and cell are thermostatically controlled to $\pm 0.1^\circ\text{C}$ at about 70°C , and are surrounded by a single layer of magnetic shielding. A single magnetic shield is sufficient, since the transition of interest is independent of magnetic field to first order.

The absorption cell is illuminated by the emission from a single-mode diode laser, Mitsubishi ML-4001, that is tuned to one of the ^{87}Rb D_1 hyperfine resonance lines (794.7 nm); this produces a hyperfine polarization in the ground state. A microwave field is either swept or modulated through the ^{87}Rb hyperfine resonance at approximately 6834 MHz, and the ensuing change in the light transmitted through the absorption cell is monitored by a silicon photodiode.

The experimental apparatus is configured in two different ways, depending upon whether we are measuring the light shift or the line shape. These two configurations are represented in Fig. 1 by the two switch positions "A" and "B." These are not physical switches, but are displayed in the figure in order to facilitate the understanding of our set-up. The rationale behind using two different configurations was simply experimental convenience. The voltage-controlled crystal oscillator (VCXO) frequencies shown in Fig. 1 are not crucial, but are what we had available to perform the different measurements.

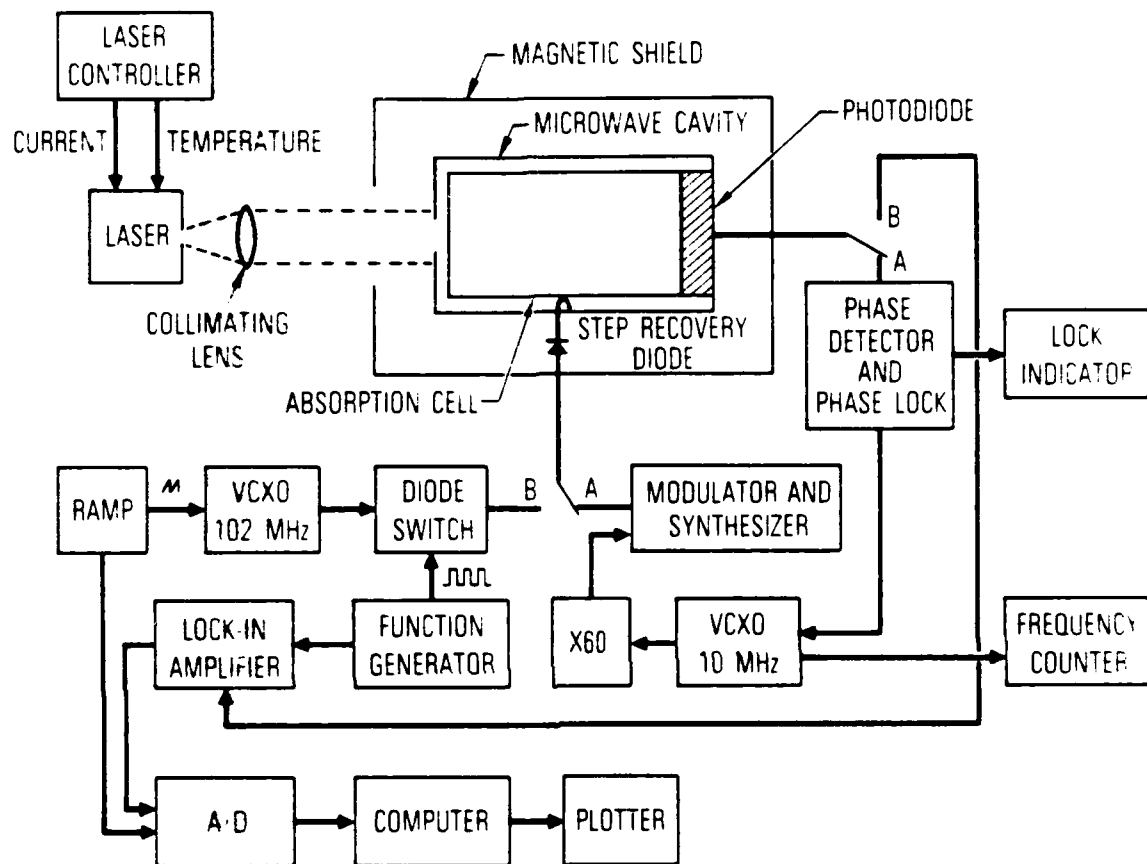


Fig. 1. Experimental Arrangement. Switch positions A and B correspond to the arrangements used to measure the light shift and line shape, respectively.

In measuring the magnitude of the light shift, one needs to determine, to a high degree of precision, the center of the optically detected hyperfine line as a function of the intensity and spectral detuning of the pumping radiation. To perform this measurement, we frequency-lock a nominal 10-MHz VCXO to the peak of the hyperfine transition line. This is schematically displayed in Fig. 1 when the switches are in the "A" position. The output frequency of the VCXO is multiplied up to 60 MHz by means of standard circuitry, and then by a "step-recovery" diode⁹ to 6840 MHz in the microwave cavity. Since this is not the proper frequency for inducing hyperfine transitions, a synthesizer is used to provide a frequency of approximately 5 MHz, which is subtracted from the 6840 MHz to yield the correct hyperfine resonance frequency. By phase-modulating the microwave radiation, an error signal generated at the photodiode is fed back to the VCXO. This scheme is similar to the typical method for locking a VCXO to the atomic transition in a Rb frequency standard.¹⁰ The VCXO frequency is averaged for 100 s, and then read with a frequency counter. From the circuitry, the relationship between the VCXO frequency and the microwave frequency is known. With this calibration we are able to determine the hyperfine resonance's peak frequency to about 1 Hz.

The line shape of the optically detected hyperfine transition is measured by ramping the frequency of a VCXO through the hyperfine resonance and monitoring the light transmitted through the absorption cell. We employ a linear VCXO that has been carefully calibrated, allowing us to convert VCXO voltage directly to frequency. The microwave field is chopped with a diode switch at a few Hz, and a lock-in amplifier is used to enhance the signal-to-noise ratio on each sweep. Typically, 16 repetitive scans, taking about 2 min each, are averaged with the aid of an HP 9825 computer. We estimate an accuracy of about 5 Hz in the line shapes with this method.

We do not have a direct measure of the strength of the microwave field in the cavity. Multiplication up to the microwave frequency from the nominal VCXO frequency is accomplished using a "step-recovery" diode. Ideally, the microwave power in the N^{th} harmonic is expected to be⁹

$$P_N = P_0/N \quad (1)$$

where P_0 is the input power to the step-recovery diode. However, the coupling coefficients between the diode and the cavity antenna, and between the cavity antenna and the cavity, will modify Eq. (1). We believe that a reasonable estimate of the microwave power in the cavity is on the order of $10 \mu\text{W}$.

The spectral linewidth of the ML 4001 diode laser, measured with a Fabry-Perot interferometer, was found to be about 100 MHz. The laser's wavelength could be tuned to either of the Doppler-broadened hyperfine absorption lines, $\Delta\nu_D \sim 500$ MHz, by varying either the diode temperature or the injection current. The diode laser is heat-sunk into a copper block whose temperature is stabilized and controlled by a thermistor in one leg of a bridge circuit that controls the current through a solid-state thermoelectric device. In this manner the diode laser's center frequency can be held to less than 100 MHz of the center of the hyperfine absorption line for about 30 min without active stabilization of the laser diode.

Typically, the laser is tuned by first adjusting the temperature so that the lasing wavelength is near the Rb D_1 line at 794.7 nm. The injection current is then used as a fine control to tune the laser over the hyperfine absorption spectrum, and as long as lasing mode hops do not occur, the injection current can be calibrated to the lasing frequency. This is found to be approximately 16 GHz/mA. Since the laser's single-mode output power is a function of the injection current, the laser power will vary as the laser is tuned. However, the fractional change in power is found to be only about 1% as the laser is tuned over several GHz, and thus the variations in laser power are neglected for these measurements. The typical total laser power in the single-mode line is found to be about 3 mW in a Gaussian beam diameter of ~ 0.45 cm.

III. RESULTS

The transmission of the laser diode emission as a function of the laser's frequency is shown in Fig. 2, along with a labeling of the observed transitions. Doppler broadening prevented resolution of the excited-state hyperfine structure, except for the ^{87}Rb transitions: $5S_{1/2}(F=1) - 5P_{1/2}(F=1, 2)$. By pumping the high-frequency component of these transitions, the effects of ^{85}Rb absorption were minimized, and except where noted all detunings are referenced with respect to this component.

A. LIGHT-SHIFT MEASUREMENTS

The light shift can be interpreted as being due to either non-energy-conserving virtual transitions,¹¹ or as the interaction between the induced polarization of the atom and the electric field of the light.¹² Both of these interpretations are consistent with second-order perturbation theory, which predicts a linear relationship between the shift and the light intensity. In either case, one can show that the light shift can be expressed qualitatively as

$$\Delta\nu_{\text{hfs}} \sim \pm I_0 \frac{(\nu_0 - \nu_L)}{[(\nu_0 - \nu_L)^2 + (\frac{1}{2\pi\tau})^2]} \quad (2)$$

where constants have been omitted for clarity. The plus and minus signs refer to excitation from the lower or upper ground-state hyperfine level, respectively. The incident-light intensity is denoted by I_0 , the atomic transition frequency is denoted by ν_0 , the laser emission frequency is ν_L , and τ is the spontaneous lifetime of the excited state.

Our results, shown in Fig. 3, of the light shift versus incident-laser intensity are markedly different from the strict linear dependence predicted by the above expression. From top to bottom, the four curves represent laser detunings of approximately -400 MHz, -200 MHz, 0, and +200 MHz. All of these curves show the same general behavior: they are linear at low laser intensity, reach an extremum, and finally saturate to a light-shift value that

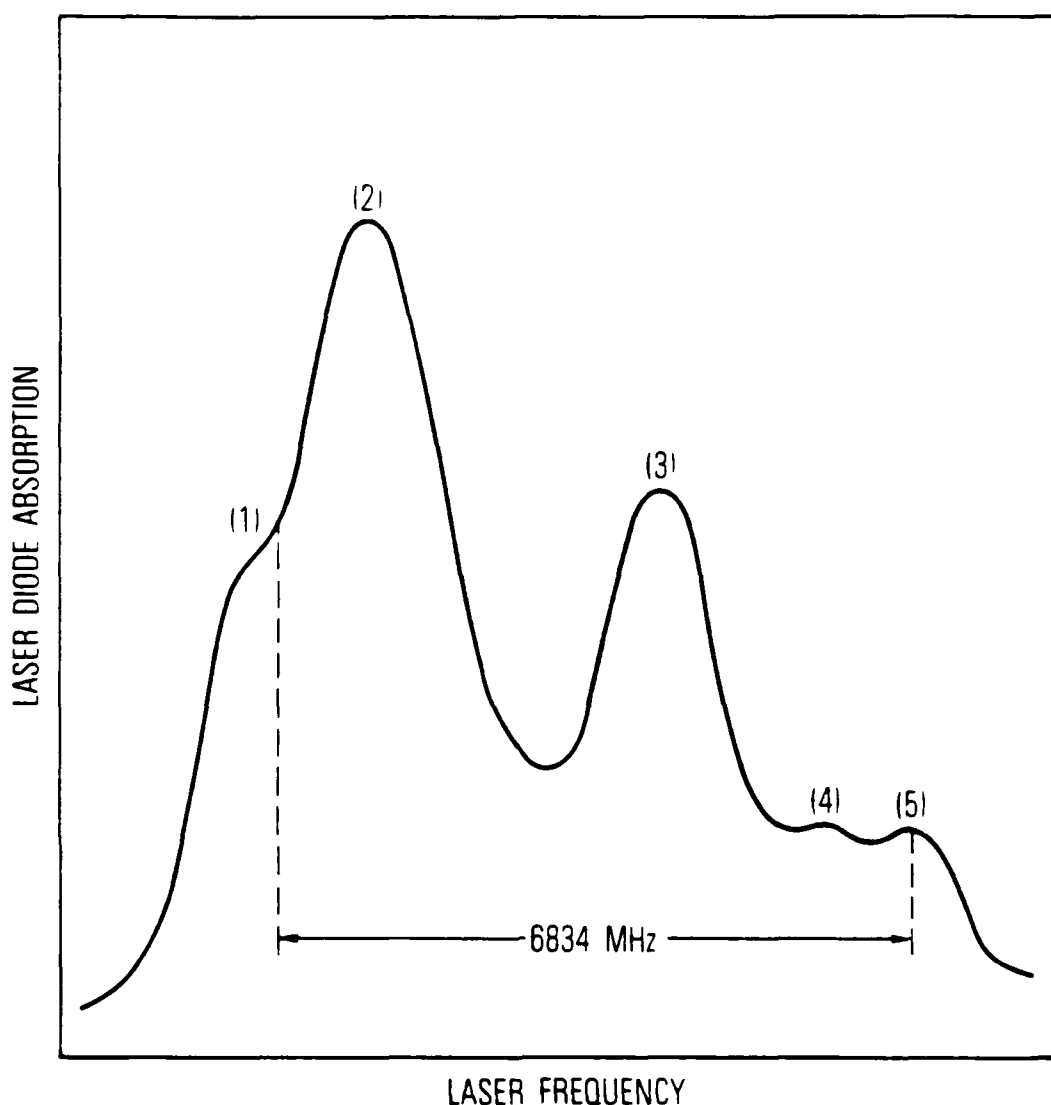


Fig. 2. Rb Hyperfine Transitions Observed in Transmission of the Laser Light. The numbered resonances correspond to the following transitions:

- (1) ^{87}Rb : $5^2\text{S}_{1/2}(\text{F} = 2) - 5^2\text{P}_{1/2}(\text{F} = 1, 2)$
- (2) ^{85}Rb : $5^2\text{S}_{1/2}(\text{F} = 3) - 5^2\text{P}_{1/2}(\text{F} = 2, 3)$
- (3) ^{85}Rb : $5^2\text{S}_{1/2}(\text{F} = 2) - 5^2\text{P}_{1/2}(\text{F} = 2, 3)$
- (4) ^{87}Rb : $5^2\text{S}_{1/2}(\text{F} = 1) - 5^2\text{P}_{1/2}(\text{F} = 1)$
- (5) ^{87}Rb : $5^2\text{S}_{1/2}(\text{F} = 1) - 5^2\text{P}_{1/2}(\text{F} = 2)$

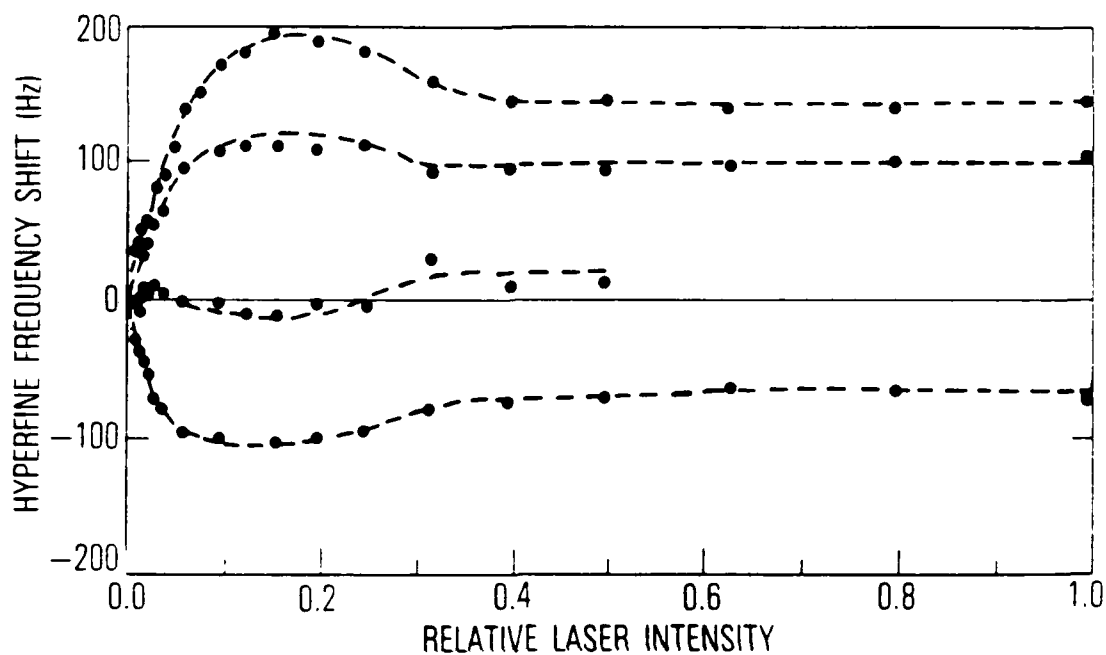


Fig. 3. Experimental Results of Light Shift versus Incident Laser Intensity. From top to bottom the curves represent laser detunings of approximately -400, -200, 0, and +200 MHz.

seems to depend only on the laser detuning from the atomic resonance. The slight light shift observed when the laser is tuned on resonance can be easily explained by the partial overlap of the $5S_{1/2}(F=1) - 5P_{1/2}(F=1, 2)$ transitions.

The linearity of these curves at low light intensity, and the sign of their symmetry about zero-frequency detuning, are consistent with the above expression. However, Eq. (2) does not predict either the extrema or the saturation regions in the light-shift curves. The extrema and saturation regions are also not consistent with a dressed atom model of the light shift which predicts a square-root dependence of the shift on high light intensity,¹³ as demonstrated by Liao and Bjorkholm.² In order to understand this discrepancy more fully, we undertook a second set of experiments to analyze the line shape of the microwave resonances as a function of laser intensity and tuning.

B. LINE SHAPE MEASUREMENTS

In Fig. 4 we present representative samples of our microwave line shape measurements. The upper line shapes correspond to low incident-laser intensity, $\sim 0.5 \text{ mW/cm}^2$, for several different detunings of the laser frequency. From left to right these are -420 , 0 , and $+420 \text{ MHz}$. The lower curves were observed with full laser intensity, $\sim 10 \text{ mW/cm}^2$. From the figure it is apparent that for higher laser intensities the microwave line shape is asymmetric when the laser is tuned off resonance, and that this asymmetry has the same sign as the light shift.

To summarize, then, we find that with high laser power the light shift has a nonlinear dependence on light intensity, and that this nonlinearity appears to be connected with an optically induced asymmetry in the microwave line shape. From these observations one might be tempted to assume that these effects are due to the onset of dynamic Stark splitting. (In our experiment $\Omega\tau \sim 0.1$, where Ω is the optical Rabi frequency.) However, the nonlinearity does not have the expected square-root dependence, and the sign of the microwave asymmetry is wrong: for an unresolved splitting one would predict two asymmetric resonances shifting away from one another with increasing laser

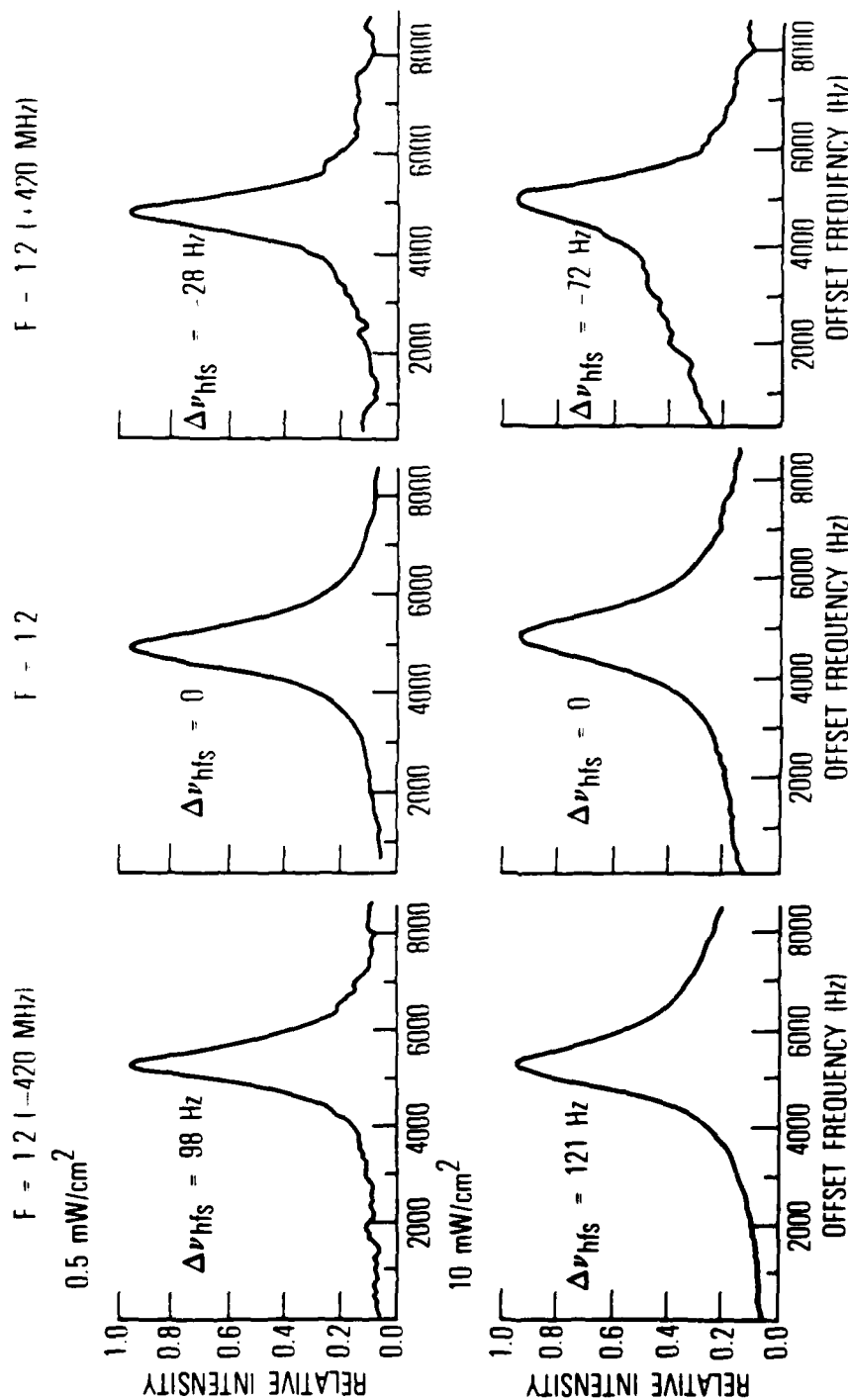


Fig. 4. Experimental Results of the Microwave Line Shape Measurements. The top row is for low laser intensity, $\sim 0.5 \text{ mW/cm}^2$, and the bottom row for high laser intensity, $\sim 10 \text{ mW/cm}^2$. From left to right the laser detunings are -420 , 0 , and $+420 \text{ MHz}$.

intensity,¹⁴ so that the sign of the asymmetry would be opposite that of the observed light shift. In the following section we show that these effects can be adequately described by the inhomogeneous light shift, which does not necessarily include the phenomenon of dynamic Stark splitting.

IV. MODEL OF THE INHOMOGENEOUS LIGHT SHIFT

In general, different atoms in a gas experience different local perturbations of their atomic states. For the hyperfine states of ^{87}Rb , as shown in Fig. 5, the differences are usually the result of gradients over the cell dimensions: temperature gradients, static magnetic-field gradients, microwave energy-density gradients, light-intensity gradients, etc. If these gradients are large enough, and if the atom cannot average over them, then the hyperfine transition will be inhomogeneously broadened.

In an attempt to model these inhomogeneous effects, consider a cylindrical cell divided into a number of finely spaced layers, where protruding through each layer are a number of finely spaced volume elements. We assume that the atoms within a volume element all experience the same perturbations, and can be described by a local density matrix determined by rate equations similar to those used by Missout and Vanier:¹⁵

$$\dot{\rho}(r, \theta, z) = \dot{\rho}(r, \theta, z)_{\text{relax}} + \dot{\rho}(r, \theta, z)_{\text{rf}} + \dot{\rho}(r, \theta, z)_{\text{opt}} \quad (3)$$

The three terms on the right-hand side of Eq. (3) correspond to the effects of relaxation, the microwave field, and optical excitation, respectively; each of these will be discussed more fully below. In addition, we assume that the microwave transition is Dicke narrowed,¹⁶ so that Doppler effects in the microwave spectra can be ignored.

The local density matrix determines the fraction of light transmitted by a particular volume element. Rows of these volume elements determine the fraction of incident light transmitted by the cell. We perform the calculation by first considering a particular row. We assume we know the light intensity incident on this row, and average it over the row's cross-sectional area. We also assume that we know the microwave magnetic field strength at any point along the row, and average it over a given volume element. We can then step through the row of volume elements, calculating the average

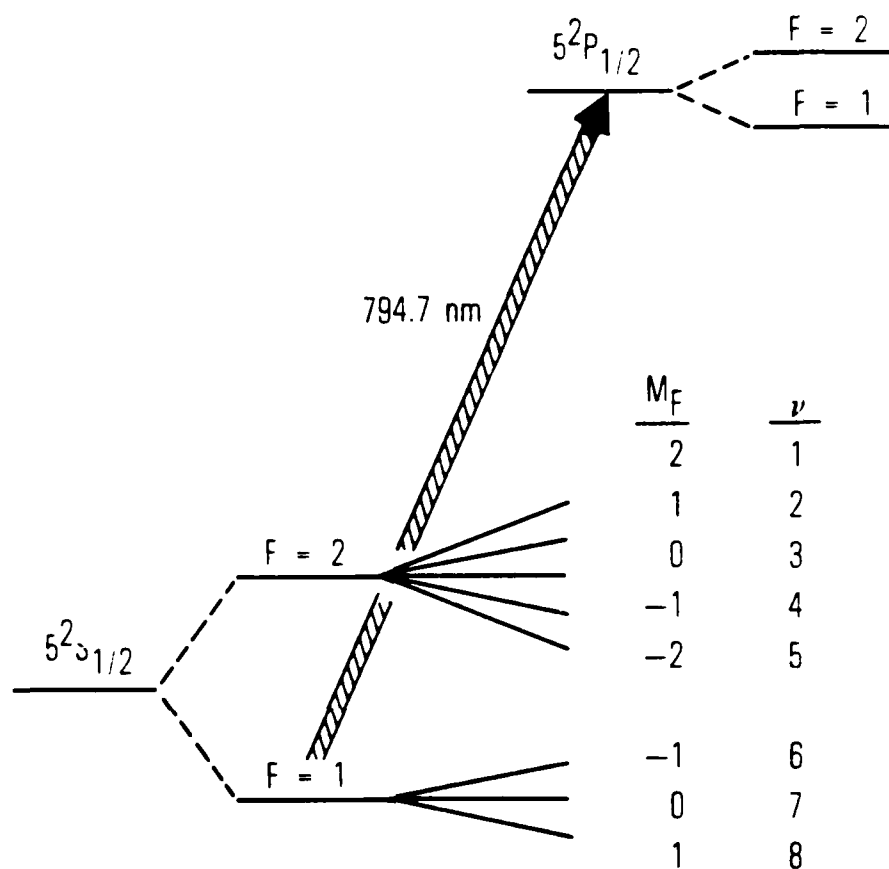


Fig. 5. Schematic Energy Level Diagram of ^{87}Rb .

light-intensity attenuation for each step. In this way we can determine the light intensity transmitted through the cell as a function of microwave frequency, thus obtaining the microwave line shape.

Once the line shape has been calculated, it is a relatively simple matter to determine the frequency corresponding to the peak of the line shape; this is the frequency that is measured in our experiments. We should note that this is equivalent to determining the resonant frequency for the homogeneous packet of atoms that has the greatest contribution to the line shape. When local perturbations differ significantly from one another, we refer to the dependence of this resonant frequency on the incident-light intensity as the inhomogeneous light shift, in order to distinguish it from the more fundamental light shift discussed by Happer and Mathur.⁵

A. THE LOCAL DENSITY MATRIX

The first term in Eq. (3) refers to uniform relaxation of the density matrix. Since our present interest is in the effects of light-intensity gradients, we assume that the rate constants for this term are independent of spatial position within the cell. Following Missout and Vanier,¹⁵ we express this term as

$$[\dot{\rho}_{vv}(r, \theta, z)]_{\text{relax}} = -\gamma_1 \left[\frac{1}{8} - \rho_{vv}(r, \theta, z) \right] \quad (4)$$

$$[\dot{\rho}_{vv'}(r, \theta, z)]_{\text{relax}} = \gamma_2 \rho_{vv'}(r, \theta, z) \quad (v \neq v') \quad (5)$$

where we have assumed that only two rates are necessary to describe the relaxation of the ground-state multiplets γ_1 and γ_2 , which refer to the longitudinal and transverse relaxation rates, respectively.

The second term of Eq. (3) describes the coherences produced in the density matrix as a result of the application of microwaves at the hyperfine transition frequency. Since the cell is situated in a TE_{111} microwave cavity, this term will have a very sensitive dependence on spatial position. We will simplify our calculation by assuming that the only coherence generated in the

density matrix is between the (F, m_F) $(2,0) - (1,0)$ states. Since the Zeeman splitting is ~ 100 times larger than the width of the observed line shapes, our assumption corresponds quite closely to our experimental situation. Thus, we only need to consider the terms

$$[\dot{\rho}_{77}(r, \theta, z)]_{\text{rf}} = 2\omega_1(r, \theta, z) \text{Im} [\rho_{37}(r, \theta, z)e^{i\omega t}] \quad (6)$$

$$[\dot{\rho}_{33}(r, \theta, z)]_{\text{rf}} = -2\omega_1(r, \theta, z) \text{Im} [\rho_{37}(r, \theta, z)e^{i\omega t}] \quad (7)$$

$$\begin{aligned} [\dot{\rho}_{37}(r, \theta, z)]_{\text{rf}} &= i\omega_1(r, \theta, z)[\rho_{33}(r, \theta, z) - \rho_{77}(r, \theta, z)]e^{-i\omega t} \\ &\quad - i\omega_0\rho_{37}(r, \theta, z) \end{aligned} \quad (8)$$

where ω_0 is the unperturbed hyperfine resonance frequency, and $\omega_1(r, \theta, z)$ is the spatially dependent microwave Rabi frequency.

The last term in Eq. (3) corresponds to the optical pumping process. This term has a radial dependence that results from the intensity profile of the laser beam, and an axial and angular dependence that results from optical absorption by successive layers of Rb atoms in the cell. Since the laser linewidth is much narrower than the hyperfine splitting, but much broader than the Zeeman splitting, the laser pumps atoms out of only one hyperfine state, but out of all Zeeman sublevels of that state equally. As shown in Fig. 5, we consider the optical transitions $5S_{1/2}(F=1) - 5P_{1/2}(F=1, 2)$, so that from Missout and Vanier¹⁵ we have

$$\begin{aligned} [\dot{\rho}_{\nu\nu}(r, \theta, z)]_{\text{opt}} &= -\Gamma(r, \theta, z)\rho_{\nu\nu}(r, \theta, z)\delta_{\mu\nu} \\ &\quad + \frac{\Gamma(r, \theta, z)}{8} \sum_{\mu} \rho_{\mu\mu}(r, \theta, z) \quad (\mu = 6, 7, 8) \end{aligned} \quad (9)$$

$$\dot{\rho}_{37}(r, \theta, z)_{\text{opt}} = -\left[\frac{\Gamma(r, \theta, z)}{2} + i\delta\omega(r, \theta, z)\right] \rho_{37}(r, \theta, z) \quad (10)$$

where $\Gamma(r, \theta, z)$ and $\delta\omega(r, \theta, z)$ are the spatially dependent pumping rate and light shift, respectively.

Two important assumptions are made in writing Eqs. (9) and (10). First, because of the presence of a significant amount of nitrogen in our cell, we assume that relaxation from the P state is predominantly nonradiative,¹⁷ and that it occurs with equal probability to all of the ground-state sublevels. Second, since the optical Rabi frequencies that we achieve in our experiment are much smaller than the relaxation rate from the excited P state, we assume there is negligible mixing of the ground and excited states. Thus, this model of the inhomogeneous line shape is essentially a low-light-intensity model.

Since we are only concerned with relatively low light intensities, we expect the light shift to be proportional to the light intensity at any point in the cell, as predicted by second-order perturbation theory. This is quite convenient for our computation, since we need only calculate, using the theory of Happer and Mathur,^{3,5} the light shift once. However, this will only be correct if the spectral line shape of the laser does not change as the beam propagates through the cell.^{3,5} In the present experiment, the optical absorption line is Doppler broadened to ~500 MHz, so that we wouldn't expect the ~100 MHz laser line to experience any appreciable distortion as it passes through the vapor.

From the symmetry of our model it is apparent that

$$\rho_{11} = \rho_{22} = \rho_{44} = \rho_{55} \quad ; \quad \rho_{66} = \rho_{88} \quad (11)$$

Thus, we need only consider solutions to the following equations:

$$\dot{\rho}_{11}(r, \theta, z) = \frac{\Gamma(r, \theta, z)}{8} \sum_{\mu} \rho_{\mu\mu}(r, \theta, z) + \gamma_1 \left[\frac{1}{8} - \rho_{11}(r, \theta, z) \right] \quad (12)$$

$$\begin{aligned}\dot{\rho}_{33}(r, \theta, z) = & \frac{\Gamma(r, \theta, z)}{8} \sum_{\mu} \rho_{\mu\mu}(r, \theta, z) + \gamma_1 \left[\frac{1}{8} - \rho_{33}(r, \theta, z) \right] \\ & - 2\omega_1(r, \theta, z) \operatorname{Im} [\rho_{37}(r, \theta, z) e^{i\omega t}] \end{aligned} \quad (13)$$

$$\begin{aligned}\dot{\rho}_{66}(r, \theta, z) = & -\Gamma(r, \theta, z) \rho_{66}(r, \theta, z) + \frac{\Gamma(r, \theta, z)}{8} \sum_{\mu} \rho_{\mu\mu}(r, \theta, z) + \\ & \gamma_1 \left[\frac{1}{8} - \rho_{66}(r, \theta, z) \right] \end{aligned} \quad (14)$$

$$\begin{aligned}\dot{\rho}_{77}(r, \theta, z) = & -\Gamma(r, \theta, z) \rho_{77}(r, \theta, z) + \frac{\Gamma(r, \theta, z)}{8} \sum_{\mu} \rho_{\mu\mu}(r, \theta, z) + \\ & \gamma_1 \left[\frac{1}{8} - \rho_{77}(r, \theta, z) \right] + 2\omega_1(r, \theta, z) \operatorname{Im} [\rho_{37}(r, \theta, z) e^{i\omega t}] \end{aligned} \quad (15)$$

$$\begin{aligned}\dot{\rho}_{37}(r, \theta, z) = & -\left[\left(\frac{\Gamma(r, \theta, z)}{2} + \gamma_2 \right) + i(\omega_0 + \delta\omega(r, \theta, z)) \right] \rho_{37}(r, \theta, z) + \\ & i\omega_1(r, \theta, z) [\rho_{33}(r, \theta, z) - \rho_{77}(r, \theta, z)] e^{-i\omega t} \end{aligned} \quad (16)$$

where $\mu = 6, 7, 8$.

If we assume a solution for $\rho_{37}(r, \theta, z)$ of the form $\tilde{\rho}_{37}(r, \theta, z) e^{-i\omega t}$, where $\tilde{\rho}_{37}(r, \theta, z)$ may be a slowly varying function of time, then in steady-state we have

$$\operatorname{Im} [\rho_{37}(r, \theta, z) e^{i\omega t}] = \omega_1(r, \theta, z) c(r, \theta, z) [\rho_{33}(r, \theta, z) - \rho_{77}(r, \theta, z)] \quad (17)$$

where we call $c(r, \theta, z)$ the local line shape factor; i.e.,

$$c(r, \theta, z) = \frac{\left[\frac{\Gamma(r, \theta, z)}{2} + \gamma_2 \right]}{\left\{ \left[\frac{\Gamma(r, \theta, z)}{2} + \gamma_2 \right]^2 + [\omega - \omega_0 - \delta\omega(r, \theta, z)]^2 \right\}} \quad (18)$$

Using Eq. (17) in Eqs. (12) through (15) we can, after some algebra, obtain analytical expressions for the local steady-state density matrix elements:

$$\rho_{77}(r, \theta, z) = \frac{\gamma_1 [\gamma_1 + 4\omega_1^2(r, \theta, z) c(r, \theta, z)]}{\Lambda(r, \theta, z)} \quad (19)$$

$$\rho_{33}(r, \theta, z) = \rho_{77}(r, \theta, z) + \frac{\gamma_1 \Gamma(r, \theta, z)}{\Lambda(r, \theta, z)} \quad (20)$$

$$\rho_{66}(r, \theta, z) = \frac{1}{2} \left[\frac{\Gamma(r, \theta, z) \rho_{77}(r, \theta, z) + \gamma_1}{3\Gamma(r, \theta, z) + 4\gamma_1} \right] \quad (21)$$

$$\rho_{11}(r, \theta, z) = \frac{1}{8} + \left[\frac{\Gamma(r, \theta, z)}{4\gamma_1} \right] \rho_{66}(r, \theta, z) + \left[\frac{\Gamma(r, \theta, z)}{8\gamma_1} \right] \rho_{77}(r, \theta, z) \quad (22)$$

where

$$\begin{aligned} \Lambda(r, \theta, z) = & 4\omega_1^2(r, \theta, z) c(r, \theta, z) \left[\Gamma(r, \theta, z) + 8\gamma_1 + \frac{\Gamma^2(r, \theta, z)}{\Gamma(r, \theta, z) + \gamma_1} \right] + \\ & \gamma_1 [5\Gamma(r, \theta, z) + 8\gamma_1] \end{aligned} \quad (23)$$

B. THE MICROWAVE RABI FREQUENCY

In order to determine explicitly the local density matrix elements, it is necessary to have an expression for the local Rabi frequency. Since we are only considering the 0-0 hyperfine transition, the Rabi frequency is given by

$$\omega_1(r, \theta, z) = \frac{\pi \mu_0}{h} B_z(r, \theta, z) \quad (24)$$

where μ_0 is the Bohr magneton and B_z is the axial component of the microwave magnetic field. For a TE_{111} cavity, this field component has the form¹⁸

$$B_z(r, \theta, z) = B_0 J_1\left(\frac{1.841r}{R}\right) \cos\theta \sin\left(\frac{\pi z}{L}\right) \quad (25)$$

where R and L are the cavity radius and length, respectively. The field amplitude B_0 can be related to the energy density in the cavity,¹⁸ and thus to the cavity Q and power loss. After performing the necessary algebra, we have for the local Rabi frequency

$$\omega_1(r, \theta, z) = \frac{\pi \mu_0}{h} \left[\frac{(1 - \lambda^2/4L^2)}{\pi R^2 L} \frac{4Q \langle P \rangle}{(0.236)\nu_0} \right]^{1/2} J_1\left(\frac{1.841r}{R}\right) \cos\theta \sin\left(\frac{\pi z}{L}\right) \quad (26)$$

where $\langle P \rangle$ is the rms microwave power supplied to the cavity.

Averaging Eq. (26) over the volume element $r\delta r\delta\theta\delta z$, we have, for the average local Rabi frequency used in the calculation, the following:

$$\langle \omega_1(r, \theta, z) \rangle = \kappa \left[\frac{4L \sin(\delta\theta/2) \sin(\frac{\pi\delta z}{2L})}{\pi r \delta r \delta\theta \delta z} \right] \cos\theta \sin\left(\frac{\pi z}{L}\right) \times$$

$$\sum_{n=0}^{\infty} A_n \left[\left(r + \frac{\delta r}{2}\right)^{2n+3} - \left(r - \frac{\delta r}{2}\right)^{2n+3} \right] \quad (27)$$

where

$$\kappa = \frac{\pi \mu_0}{h} \left[\frac{1 - \lambda^2/4L^2}{\pi R^2 L} \frac{4Q \langle P \rangle}{(0.236)\nu_0} \right]^{1/2} \quad (28)$$

and

$$A_n = (-1)^n \left(\frac{1.841}{R}\right)^{2n+1} [2^{2n+1} (2n+3) n! (n+1)!]^{-1} \quad (29)$$

C. THE PUMPING RATE AND LIGHT SHIFT

Both the pumping rate and light shift are functions of the light intensity and spectral overlap of the laser line and Doppler-broadened absorption line. In particular, we have for the local pumping rate

$$\Gamma(r, \theta, z) = \frac{2\pi}{h\nu_L} \int I(r, \theta, z, \nu) \sigma_D(\nu) d\nu \quad (30)$$

where ν_L is the center frequency of the laser. For convenience, we will assume that the laser line is Gaussian,¹⁹ so that

$$I(r, \theta, z, \nu) = I(r, \theta, z) \frac{4}{\Delta\nu_L} \left[\frac{\ln 2}{\pi} \right]^{1/2} \exp\left[-4\ln 2 \left(\frac{\nu - \nu_L}{\Delta\nu_L} \right)^2 \right] \quad (31)$$

where $\Delta\nu_L$ is the laser linewidth and $I(r, \theta, z)$ is the total local intensity. Using Eq. (31) in (30) we have, for the local pumping rate,

$$\Gamma(r, \theta, z) = I(r, \theta, z) \frac{4\pi r_0^2 f c}{h\nu_0} \left[\frac{\pi \ln 2}{\Delta\nu_L^2 + \Delta\nu_D^2} \right]^{1/2} \exp\left[-4\ln 2 \left(\frac{\delta\nu^2}{\Delta\nu_L^2 + \Delta\nu_D^2} \right) \right] \quad (32)$$

where ν_0 is the center frequency of the optical absorption line; $\Delta\nu_D$ is the absorption linewidth; $\delta\nu$ is the detuning of the laser from the absorption line; and r_0 , f , and c are, respectively, the classical electron radius, the oscillator strength of the transition, and the speed of light.

From our measurements we can approximate the laser with a Gaussian radial intensity distribution at the entrance of the cell:

$$I(r, \theta, 0) = \frac{4\ln 2}{\pi a^2} P_0 \exp\left[-4\ln 2 (r/a)^2 \right] \quad (33)$$

where a is the Gaussian beam diameter and P_0 is the total power in the beam. We average Eq. (33) over an arbitrary row's cross-sectional area, which gives

$$\langle I(r, \theta, 0) \rangle = \frac{4\ln 2}{\pi a^2} P_0 \exp\left[-4\ln 2 (r/a)^2 \right] [1 - \ln 2 (\delta r/a)^2] \quad (34)$$

As the beam propagates through a row in the cell, each volume element attenuates the beam by an amount $\langle \Delta I(r, \theta, z) \rangle_1$. Thus, the average local intensity at the n^{th} volume element of a particular row is

$$\langle I(r, \theta, z) \rangle_n = \langle I(r, \theta, 0) \rangle - \sum_{i=1}^{n-1} \langle \Delta I(r, \theta, z) \rangle_i \quad (35)$$

If we assume exponential attenuation of the light as it passes through the vapor, then

$$\langle \Delta I(r, \theta, z) \rangle_i = - \eta_i [Rb] \langle \Gamma(r, \theta, z) \rangle_i \frac{h\nu_0}{2\pi} \delta z \quad (36)$$

where η_i is the average fraction of atoms in the i^{th} volume element which can absorb light, so that

$$\eta_i = \langle \rho_{66}(r, \theta, z) \rangle_i + \langle \rho_{77}(r, \theta, z) \rangle_i + \langle \rho_{88}(r, \theta, z) \rangle_i \quad (37)$$

Equation (35) can thus be used in Eq. (32) to compute the average local pumping rate in the n^{th} volume element, and also the average local light shift for the volume element:

$$\langle \delta\omega(r, \theta, z) \rangle_n = \delta\omega_0 \left[\langle I(r, \theta, z) \rangle_n \frac{\pi a^2}{P_0 4\ell n^2} \right] \quad (38)$$

where $\delta\omega_0$ is the light shift corresponding to a light intensity of $\frac{P_0 4\ell n^2}{\pi a^2}$.

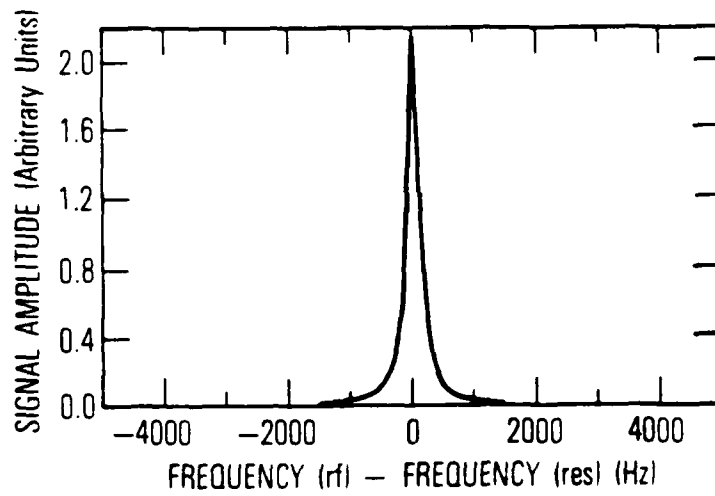
V. DISCUSSION

In order to obtain a clear picture of the inhomogeneous light shift, we have performed two sets of calculations. In the first, we consider the inhomogeneous effects in a TE_{111} microwave cavity; this should correspond closely to our experimental data. In the second set, we imagine a fictitious cavity where the microwave magnetic field strength is everywhere constant, and directed parallel to the cavity axis. Microwave line shapes and the light shift versus input laser intensity for both microwave field configurations are shown in Figs. 6 through 9. The input parameters for these calculations are listed in Table 1.

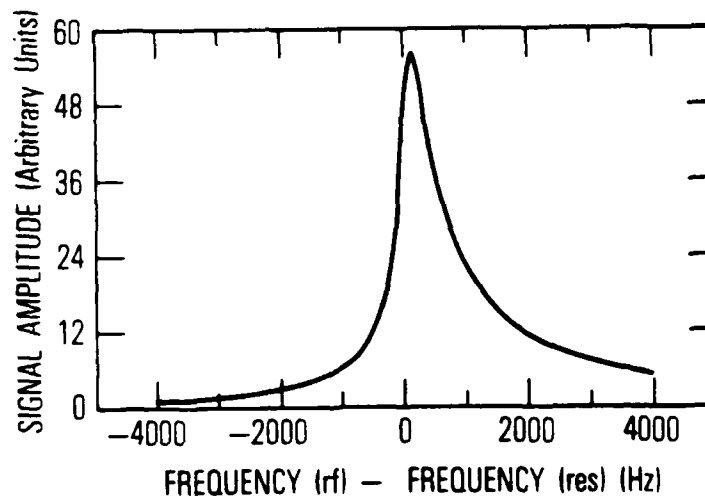
In Fig. 6 we compare the microwave line shapes calculated for a TE_{111} microwave cavity at low and high laser intensities. When the laser intensity is low, the line shape appears quite symmetric. This is because the conditions for light-induced inhomogeneous broadening, as discussed in the Appendix, are not satisfied at very low laser intensity. When the laser intensity is high, the line shape is highly asymmetric, with the asymmetry in the direction of the light shift.

The sign of the asymmetry is related to the transmission signal amplitude for the local volume elements. In the limit of high light intensity ($\Gamma \gg \omega_1$), this amplitude is proportional to $(\omega_1/\Gamma)^2$.²⁰ Thus, the homogeneous packets of atoms that experience the largest light shift contribute the least to the total signal amplitude. In the TE_{111} microwave cavity, this effect is further enhanced by the overlap of the radial components of the microwave and optical fields. The optical field has a radial distribution described by a Gaussian function, the microwave field a radial distribution described by a first-order Bessel function. Thus, for radial positions where the optical field is most intense, the microwave field is not, and vice versa.

In Fig. 7 we compare the low- and high-intensity line shapes when the microwave field is constant. Again, for low laser intensity the line shape is

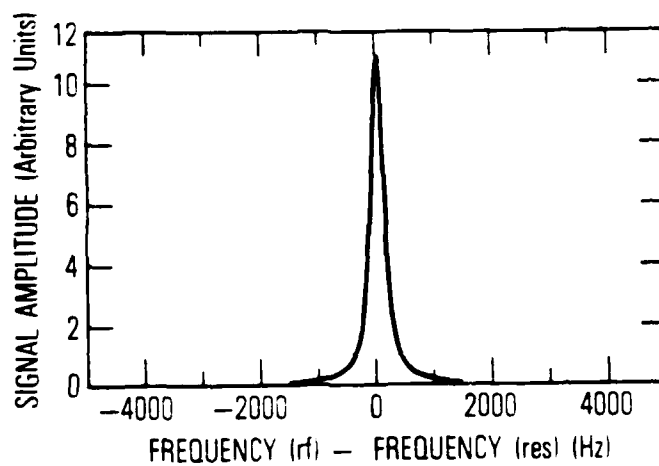


(a) $10 \mu\text{W}/\text{cm}^2$

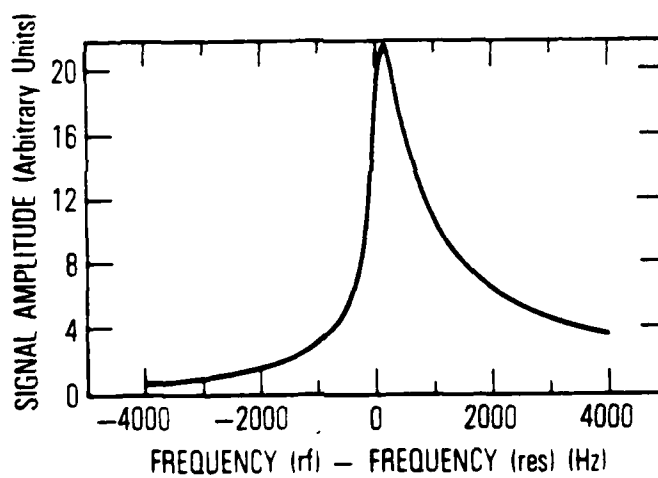


(b) $10 \text{ mW}/\text{cm}^2$

Fig. 6. Calculated Resonant Microwave Line Shapes in a TE_{111} Microwave Cavity for Low and High Laser Intensity.



(a) $10 \mu\text{W}/\text{cm}^2$



(b) $10 \text{ mW}/\text{cm}^2$

Fig. 7. Calculated Resonant Microwave Line Shapes in a Fictitious Microwave Cavity with Constant rf Magnetic Field for Low and High Laser Intensity.

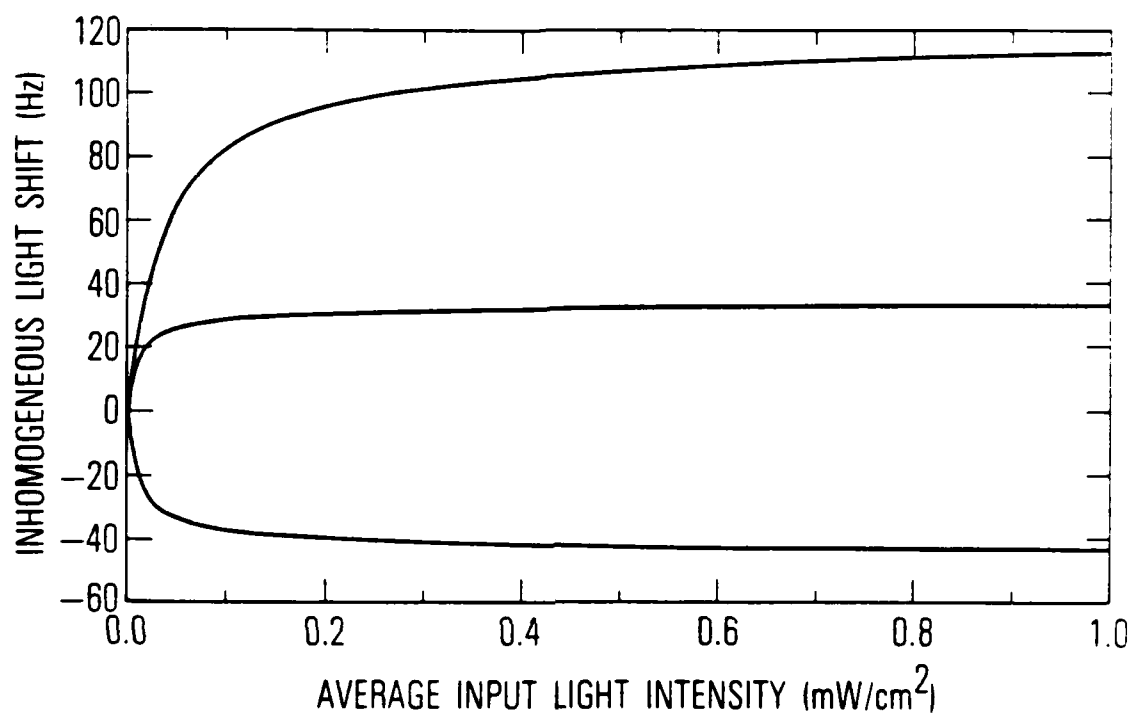


Fig. 8. Calculated Inhomogeneous Light Shift in a TE_{111} Microwave Cavity for Several Detunings of the Laser. From top to bottom these are -411, -201, and +219 MHz.

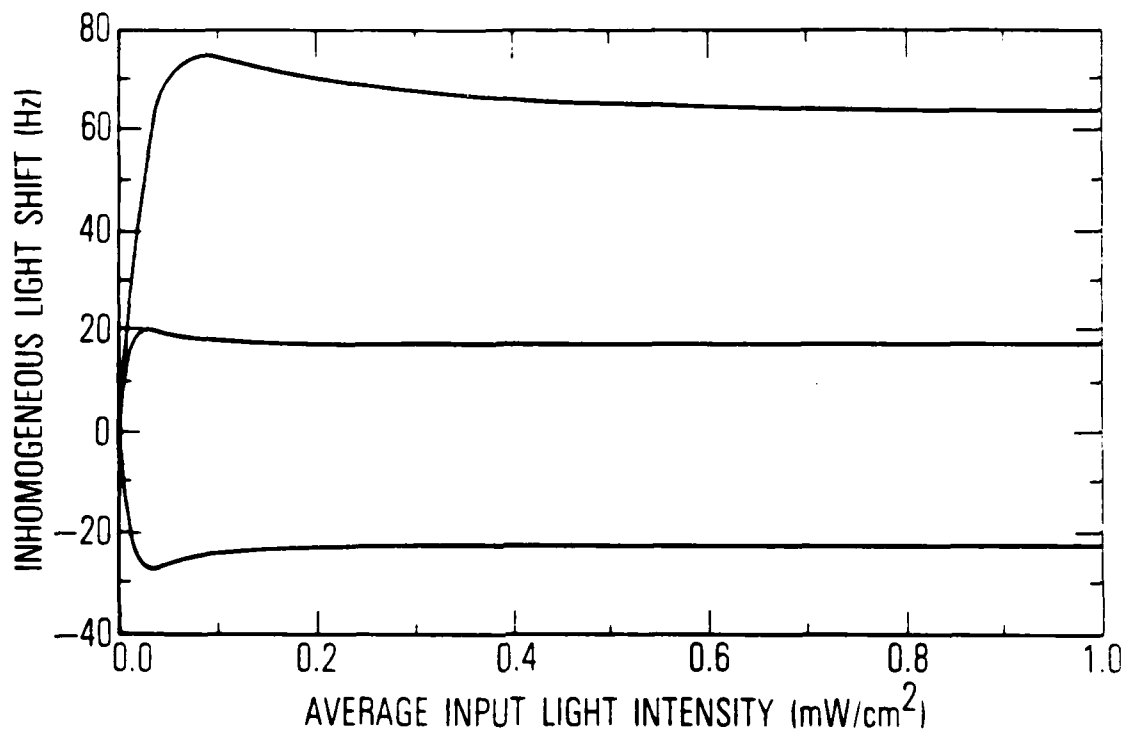


Fig. 9. Calculated Inhomogeneous Light Shift in a Fictitious Microwave Cavity with Constant rf Magnetic Field for Several Detunings of the Laser. From top to bottom these are -411, -201, and +219 MHz.

Table 1. Calculation Parameters

laser linewidth	$\Delta\nu_L = 100 \text{ MHz}$
laser beam diameter	$a = 0.45 \text{ cm}$
absorption linewidth	$\Delta\nu_D = 500 \text{ MHz}$
longitudinal relaxation rate	$\gamma_1 = 100 \text{ Hz}$
transverse relaxation rate	$\gamma_2 = 100 \text{ Hz}$
rubidium density	$[^{87}\text{Rb}] = 1 \times 10^{11} \text{ cm}^{-3}$
cell length	$L = 3.8 \text{ cm}$
cell radius	$R = 1.35 \text{ cm}$
cavity aperture diameter	$D = 1.6 \text{ cm}$
cavity quality factor	$Q = 100$
rms microwave power	$\langle P \rangle = 10 \text{ } \mu\text{W}$

*Note: In this cavity, 10 μW of rf input power implies an average axial magnetic field of approximately 9 μG .

symmetric, and at high laser intensity the line shape is asymmetric. The sign of the asymmetry is also the same as for a TE_{111} cavity, which we would expect from the arguments presented above.

In the Appendix, the necessary conditions for observing inhomogeneous broadening are discussed in terms of the dephasing rate ($1/T_2$) and the longitudinal relaxation rate ($1/T_1$). However, each of these rates is a function of both the pumping rate and the microwave Rabi frequency. Therefore, each of these rates varies spatially, and as a consequence so do the degrees to which the inhomogeneous broadening conditions are satisfied. Thus, the inhomogeneous line shape is not composed of homogeneous line shapes with equal linewidths, but of homogeneous line shapes with different linewidths, the linewidths being determined by the local T_2 's and the degree to which motional narrowing occurs on a local level.

Figure 8 shows the calculated inhomogeneous light shift as a function of incident light intensity in a TE_{111} cavity. The several curves correspond to different laser detunings, and it is apparent that the agreement between theory and experiment, shown in Fig. 3, is rather good. In Fig. 9 we show the inhomogeneous light shift for a constant microwave field. The fact that the nonlinearity is observed with both calculations implies that this feature is primarily determined by the light-intensity gradients in the cell, and not by the microwave field distribution. The puzzling thing about Figs. 8 and 9 is that, though extrema in the inhomogeneous light-shift curves were observed experimentally, such extrema are only predicted in the constant-microwave-field calculations.

The extrema in the experimental light-shift curves could be due to a number of effects not considered in our calculation. For example, the 0-0 hyperfine transition frequency has a quadratic dependence on the static magnetic field strength. Thus, magnetic field inhomogeneities could easily have a significant effect on the inhomogeneous light shift. However, a more intriguing possibility is that the atoms actually do experience a relatively constant microwave field. This might occur if motional narrowing on a local level allowed some averaging of the microwave and optical fields.

As pointed out in the Appendix, the criterion for atoms being frozen in place might not be strictly fulfilled everywhere in the cell. In such a case the microwave and optical fields might be averaged in some regions of the cell but not in others. The results of this could be to effectively change the spatial distribution of the microwave field as experienced by an atom, so that the "effective" field might have a spatial distribution quite different from that of the TE_{111} cavity. If this local motional narrowing is occurring, the extrema in the light-shift curves should be a function of the buffer gas density: as the buffer gas density is increased, the diffusion length of the atom decreases, and less averaging of the fields is possible. The effective microwave field distribution will then approach the TE_{111} distribution as the buffer density is increased, and the measured light-shift curves should approach those displayed in Fig. 8. Unfortunately, at the present time we are unable to make any definite statements as to the source of the extremum.

VI. CONCLUSIONS

We have found that inhomogeneous broadening of a spectral line as a result of light-intensity gradients can lead to a nonlinear dependence of the line shape's center frequency on incident-light intensity. Thus, one needs to be very careful in analyzing optically induced energy-level shifts, either for high-precision spectroscopy or for a determination of transition dipole matrix elements, since this nonlinearity could significantly influence the results. In addition, one should be very careful in interpreting asymmetries in resonance lines as being due to the onset of an Autler-Townes-type splitting.¹ Except for the sign, asymmetries due to inhomogeneous broadening could be easily confused with this effect. It is our contention that this was exactly the case with the asymmetries observed by Arditi and Picqué for the 0-0 hyperfine transition of cesium optically pumped by a laser diode.²¹ Since the intensities that they could have reasonably achieved with their laser diode were probably similar to ours, we believe that they too were observing the effects of inhomogeneous broadening as discussed in this report.

REFERENCES

1. For a recent review of these effects in optical spectra, see P. L. Knight and P. W. Milonni, Phys. Rep. 66 (2), 21 (1980).
2. P. F. Liao and J. E. Bjorkholm, Opt. Comm. 16 (3), 392 (1976).
3. B. S. Mathur, H. Tang, and W. Happer, Phys. Rev. 171 (1), 11 (1968).
4. J. P. Barrat and C. Cohen-Tannoudji, J. Phys. Rad. 22, 329 (1961); 22, 443 (1961).
5. W. Happer and B. S. Mathur, Phys. Rev. 163 (1), 12 (1967).
6. G. Busca, M. Tetu, and J. Vanier, Can. J. Phys. 51 (13), 1379 (1973).
7. A. Risley and G. Busca, Proc. 32nd Ann. Symp. on Freq. Control, (1978), p. 506.
8. Our apparatus is essentially a modified commercial rubidium frequency standard: FRK-L, Efratom California, Inc.
9. Hewlett-Packard Application Note 913, "Step-Recovery Diode Frequency Multiplier Design."
10. M. E. Packard and B. E. Swartz, IRE Trans. on Instr. I-22, 215 (1962).
11. J. E. Bjorkholm and P. F. Liao, "Laser Spectroscopy," in Proc. of the Second Intl. Conf., Megeve, June 23-27, 1975, Lecture Notes in Physics Vol. 43 (Springer-Verlag, Berlin-Heidelberg-New York, 1975), pp. 176-185.
12. S. Pancharatnam, J. Opt. Soc. Am. 56, 1636 (1966).
13. C. Cohen-Tannoudji, Metrologia 13, 161 (1977).
14. H. R. Gray and C. R. Stroud, Jr., Opt. Comm. 25 (3), 359 (1978).
15. G. Missout and J. Vanier, Can. J. Phys. 53, 1030 (1975).
16. R. H. Dicke, Phys. Rev. 89 (2), 472 (1953).
17. W. Happer, Rev. Mod. Phys. 44 (2), 169 (1972).
18. R. A. Waldron, Theory of Guided Electromagnetic Waves, (Van Nostrand Reinhold Co., London, 1969).

PREVIOUS PAGE
IS BLANK

19. This is simply a convenience for our calculation. Actually, the line shape of a laser diode is a Lorentzian: D. Welford and A. Mooradian, Appl. Phys. Lett. 40 (7), 560 (1982).
20. L. C. Balling, "Optical Pumping," in P. W. Goodwin, ed., Advances in Quantum Electronics, (Academic Press, New York, 1975).
21. M. Arditi and J. L. Picqué, J. Phys. B. 8 (14), L331 (1975).

APPENDIX: THE POTENTIAL FOR MOTIONAL AVERAGING OF SPATIAL INHOMOGENEITIES

As mentioned in the text, there are essentially two conditions that must be met in order to have an inhomogeneously broadened microwave line. First, the local perturbation variations must be of sufficient magnitude, so that the spread in perturbed resonant frequencies is greater than the homogeneous linewidth:

$$(\delta v_{\text{loc}}/h) > (1/T_2) \quad (\text{A1})$$

where δv_{loc} represents the variation in local perturbations, and $1/T_2$ is the homogeneous linewidth. In addition, motional narrowing should be insignificant: the individual atoms should not be able to average the local perturbations. In the present case, this last requirement would be satisfied if the atoms were not able to diffuse spatially over the effective volume of local perturbation gradients during the lifetime of the hyperfine states.

If we consider diffusion in one dimension, then during the time T_1 an atom will diffuse a length l_{dif} :

$$l_{\text{dif}} = \sqrt{DT_1} \quad (\text{A2})$$

where D is the diffusion coefficient for Rb atoms in a buffer gas. In three dimensions, we can think of the atom as diffusing through a volume $V_{\text{dif}} \sim \pi l_{\text{dif}}^3$. Thus, for motional narrowing not to occur we would want

$$V_{\text{dif}}/V_{\text{eff}} = \frac{\pi(DT_1)^{3/2}}{\pi a^2 L} \ll 1 \quad (\text{A3})$$

where a is the light beam radius and L is the cell length. In the present case, if we assume a lifetime on the order of 1 msec,

$$V_{\text{dif}}/V_{\text{eff}} \sim 5 \times 10^{-3} \quad (\text{A4})$$

which suggests that to a first approximation the Rb atoms can be considered as frozen in place as a result of the presence of 10 Torr of N_2 . Caution must be exercised here because if T_1 and T_2 vary through the cell volume, then the criterion for treating the atoms as frozen in place might not be fulfilled everywhere in the cell. In that case some local averaging of the perturbations might take place (i.e., local motional narrowing).

LABORATORY OPERATIONS

The Laboratory Operations of The Aerospace Corporation is conducting experimental and theoretical investigations necessary for the evaluation and application of scientific advances to new military space systems. Versatility and flexibility have been developed to a high degree by the laboratory personnel in dealing with the many problems encountered in the nation's rapidly developing space systems. Expertise in the latest scientific developments is vital to the accomplishment of tasks related to these problems. The laboratories that contribute to this research are:

Aerophysics Laboratory: Launch vehicle and reentry fluid mechanics, heat transfer and flight dynamics; chemical and electric propulsion, propellant chemistry, environmental hazards, trace detection; spacecraft structural mechanics, contamination, thermal and structural control; high temperature thermomechanics, gas kinetics and radiation; cw and pulsed laser development including chemical kinetics, spectroscopy, optical resonators, beam control, atmospheric propagation, laser effects and countermeasures.

Chemistry and Physics Laboratory: Atmospheric chemical reactions, atmospheric optics, light scattering, state-specific chemical reactions and radiation transport in rocket plumes, applied laser spectroscopy, laser chemistry, laser optoelectronics, solar cell physics, battery electrochemistry, space vacuum and radiation effects on materials, lubrication and surface phenomena, thermionic emission, photosensitive materials and detectors, atomic frequency standards, and environmental chemistry.

Computer Science Laboratory: Program verification, program translation, performance-sensitive system design, distributed architectures for spaceborne computers, fault-tolerant computer systems, artificial intelligence and microelectronics applications.

Electronics Research Laboratory: Microelectronics, GaAs low noise and power devices, semiconductor lasers, electromagnetic and optical propagation phenomena, quantum electronics, laser communications, lidar, and electro-optics; communication sciences, applied electronics, semiconductor crystal and device physics, radiometric imaging; millimeter wave, microwave technology, and RF systems research.

Materials Sciences Laboratory: Development of new materials: metal matrix composites, polymers, and new forms of carbon; nondestructive evaluation, component failure analysis and reliability; fracture mechanics and stress corrosion; analysis and evaluation of materials at cryogenic and elevated temperatures as well as in space and enemy-induced environments.

Space Sciences Laboratory: Magnetospheric, auroral and cosmic ray physics, wave-particle interactions, magnetospheric plasma waves; atmospheric and ionospheric physics, density and composition of the upper atmosphere, remote sensing using atmospheric radiation; solar physics, infrared astronomy, infrared signature analysis; effects of solar activity, magnetic storms and nuclear explosions on the earth's atmosphere, ionosphere and magnetosphere; effects of electromagnetic and particulate radiations on space systems; space instrumentation.

END

FILMED

9-85

DTIC